Revista Facultad de Ingeniería Universidad de Antioquia
ISSN: 0120-6230
ISSN: 2422-2844
Facultad de Ingeniería, Universidad de Antioquia

Bermúdez-Calderón, Franky Aldemar; Díaz-Morales, Hernando; Mojica-Nava, Eduardo Alirio
Distribution Systems State Estimation for Distributed Generation Re-synchronization
Revista Facultad de Ingeniería Universidad de
Antioquia, no. 85, 2017, October-December, pp. 40-52
Facultad de Ingeniería, Universidad de Antioquia

DOI: 10.17533/udea.redin.n85a05

Available in: http://www.redalyc.org/articulo.oa?id=43056414005

redin Revista Facultad de Ingeniería, No.85, pp. 40-52, 2017

Distribution Systems State Estimation for Distributed Generation Re-synchronization

Estimación de estados en sistemas de distribución para resincronización de generación distribuida

Franky Aldemar Bermúdez-Calderón*, Hernando Díaz-Morales, and Eduardo Alirio Mojica-Nava

[1]Departamento de Ingeniería Eléctrica y Electrónica, Facultad de Ingeniería, Universidad Nacional de Colombia. Carrera 45 #26-85. A. A. 055051. Bogotá, Colombia

ARTICLE INFO:

Received December 05, 2016

Accepted October 31, 2017

KEYWORDS:

Distribution system state estimation, phasor measurement units, observability analysis, distributed generation, re-synchronization, self-healing, pseudo-measurements, microgrids.

Estimación de estados en sistemas de distribución, unidades de medición fasorial, análisis de observabilidad, generación distribuida, re-sincronización, auto-restablecimiento, pseudo-medidas, microrredes.

ABSTRACT: This paper presents an application of a state estimation algorithm as a tool for re-synchronization of distributed generation in a distribution system. The estimation results can be used to operate a distributed generation in grid and off-grid mode. The estimated state variables are utilized as input data to control a Diesel generator while resynchronizing as well as for a grid mode loss predictor. The proposed state estimator, with branch currents as state variables, was solved by the weighted least squares method using singular value decomposition. To ensure the observability of the distribution system, a detailed numerical observability analysis was carried out with complex power measurements and unconventional branch current phasor measurements. In the algorithm, phasor measurement units and pseudo-measurements can be incorporated. Conditions that ensure system observability and redundancy increasing are derived when those measurements are included. The approach was tested in the IEEE 13 node test feeder, to which a distributed generation was connected for external network feeding. The algorithm shows stability, convergence, allowing the distributed generation re-synchronization to the distribution system. This feature could help improve self-healing capability in microgrids that use synchronous generators.

RESUMEN: Este trabajo presenta un algoritmo de estimación de estado diseñado para sistemas de distribución. El algoritmo de estimación se utiliza para operar una generación distribuida en modo isla o conectada a una red de distribución. Las variables de estado estimadas se utilizan para controlar un generador diésel y también para predecir las pérdidas cuando la generación distribuida trabaja conectada a la red. El estimador de estado propuesto, se resolvió por el método de mínimos cuadrados ponderados y se utilizó la descomposición en valores singulares, las variables de estado son las corrientes complejas de las ramas. Para garantizar la observabilidad en el sistema de distribución se hizo un análisis de observabilidad numérica, utilizando medidas de potencia activa y reactiva y medidas del fasor complejo de corriente. Para el algoritmo se propone utilizar unidades de medición fasorial y pseudo medidas, ya que estas medidas pueden garantizar la observabilidad de un sistema y aumentar la redundancia en el conjunto de medidas. El algoritmo se probó en el sistema de distribución IEEE de 13 nodos, a este sistema se le adicionó una generación distribuida que alimenta una red externa. Entre los principales resultados, se encontró que: el algoritmo es estable, converge muy cerca de la solución, además permite hacer la re-sincronización de la generación distribuida con la red de distribución. Esta última característica puede mejorar la capacidad de auto-restablecimiento de microrredes que utilicen generadores sincrónicos.

* Corresponding author: Franky Aldemar Bermúdez Calderón

E-mail: fraabermudezc@unal.edu.co

ISSN 0120-6230

e-ISSN 2422-2844

DOI: 10.17533/udea.redin.n85a05

1. Introduction

Distribution systems (DS) are designed to carry energy from substations to loads. Nowadays, there is also the possibility of feeding loads with distributed generation (DG) and microgrids (MGs), which can cause the state of the DS changes during operation. New technological advances in DS automation can improve the monitoring of the state of the system to increase the controllability of the entire system (1; 2). The widespread use of DG, MGs, and real time measurements suggests the implementation of a state estimator (SE) at the distribution level as a consequence of the uncertainty in DS parameters operation (3). Since the late 60's, the SE has become a key element of supervision, control and planning of power systems (4). The SE provides real time information about real power system state. In this way, energy management systems can carry out several important tasks in the system planning and operation. On the other hand, at distribution level the SE was not necessary because standards and market regulators did not require line monitoring.

Despite the fact that DS's keep radial topology, they can have DG sources connected to the networks. Additionally, the changes in the existing regulation require that utility operators improve the quality of energy delivered to customers, in order to minimize the number and duration of service interruptions (2). This suggests the need for real time information, allowing more accurately the state of DS to be modeled. Thus reliable operation and power flow control are ensured as well as regulation compliance.

In some power systems, the energy market and transactions justify the implementation of state estimators at distribution level. Additionally, the use of SE in DS helps the connection of DG and MGs. This makes it necessary to control electrical variables involved in the system joint operation. Accordingly, the SE is the backbone of the automation process, because the information that it provides characterizes completely the DS (5). This allows DS's to increase the degree of automation, improve DG synchronization and the MG self-healing capability (6).

The methodology that permits to apply an estimator at distribution level has not been developed completely (2; 7). This is mainly due to lack of redundancy in the available measurements set. Therefore, it becomes necessary to improve methods and algorithms of state estimation in DSs, to take advantage of the information that can be obtained from equipment like reclosers, sectionalizers, among others which are widely used in DS.

This work presents a state estimation algorithm for DS and distributed generation feeding an external network (DGEN). To address low rank matrices, singular value decomposition (SVD) was used. In the SE, state variables are branch current phasors; from these variables, voltage phasors are computed which are more conventional state variables. The distribution transformers were modeled through the change of the base voltage for nodes located downstream. The estimated state variables are the input data for a new algorithm that synchronizes DG to the DS. This algorithm can be used to improve the self-healing capability of MGs that use synchronous generators (8). Numerical observability analysis was conducted, to determine when a DS is observable. Thus, it is ensured SE convergence to an unique solution. This analysis suggests that phasor measurement units (PMUs) can be used in the measurement set; in this way the complex current phasor can be measured. Nowadays, PMUs have become less costly and can be used in DS and MGs (9; 10). The SE was tested in the IEEE 13 node test feeder and in an DGEN.

This paper is organized as follows: section two presents a brief introduction to state estimation. In section three the numerical observability analysis of DS's is presented, including measurements of voltage magnitude, complex power and complex current. In section four, the state estimation algorithm is developed. Section five shows the implementation of the SE in the radial IEEE 13 node test feeder and DGEN; that section also presents the results for the SE algorithm and synchronization algorithm. Finally, section six concludes the paper.

2. State Estimation

The SE is an algorithm that processes data to find an estimate of the system state variables and produces the best possible estimate of the system's true state (11). This algorithm uses a measurement set, which usually is redundant and remote. The SE is based on a linear least square estimation. In some systems, the measurement values are related with the state variables via non linear functions. Then, measurement functions must be linearized around a value that approaches the solution. Eq. (1) relates the measurement functions with the state variables.

$$z = h(x) + \eta \tag{1}$$

Where z is the $m \times 1$ measurement vector, h is the $m \times 1$ vector of nonlinear measurements function, x is the $2n \times 1$ true state vector, η is an $m \times 1$ measurement error vector, m is the number of measurements, and n is the number of nodes (12).

The probability distribution function of each component of η is usually assumed as a normal distribution. In addition,

it is assumed that the measurements are random and independent. To estimate the unknown state vector x, a weighted least squares function, presented in Eq. (2), must be minimized (13).

$$\min_x \; J(x) = \sum_{i=1}^{m} \frac{[z_i - h_i(x)]^2}{\sigma_i^2} \tag{2}$$

Here, $J(x)$ is the weighted measurement residual, σ_i is the standard deviation of each measurement and reflects meter accuracy (14). A linearized matrix formulation of (2) is given by Eq. (3),

$$\begin{aligned} \min_x \; J(x) &= ||W^{-\frac{1}{2}}(z - Hx)||^2 \\ &= ||W^{-\frac{1}{2}}\,\Delta z - W^{-\frac{1}{2}} H\,\Delta x||^2 \end{aligned} \tag{3}$$

where $[W]$ is the diagonal covariance matrix of measurement errors, $[H]$ is the Jacobian matrix of measurements functions and Δx is the deviation from the linearization point. The minimum of $J(x)$ can be found using Eq. (4). A Singular Value Decomposition (SVD) (15) of the matrix $W^{-\frac{1}{2}}H$, is found as follow:

$$W^{-\frac{1}{2}} H = U \Sigma V^T \tag{4}$$

where U is an $m \times m$ orthogonal matrix, such that ($U^T = U^{-1}$), Σ is an $m \times n$ diagonal matrix, and V is an $n \times n$ orthogonal matrix. From this SVD, (3) can be written as Eq. (5)

$$\begin{aligned} \min_x J(x) &= ||W^{-\frac{1}{2}} z - U\Sigma V^T x||^2 \\ &= ||U^T W^{-\frac{1}{2}}\,\Delta z - \Sigma V^T\,\Delta x||^2 \end{aligned} \tag{5}$$

The last expression follows from the fact that $\|Q\,x\| = \|x\|$ for any orthogonal matrix Q and any vector x. In compact form (5) is rewritten as Eq. (6).

$$\min_x J(x) = ||y - \Sigma u||^2 \tag{6}$$

where $y = U^T W^{-\frac{1}{2}}\,\Delta z$ and $u = V^T\,\Delta x$. Eq. (6) can then be expanded as Eq. (7):

$$\min_x J(x) = \left|\left| \begin{bmatrix} y_1 \\ \vdots \\ y_n \\ \vdots \\ y_m \end{bmatrix} - \begin{bmatrix} \varphi_1 & 0 & \cdots & 0 \\ 0 & \varphi_2 & \cdots & 0 \\ 0 & 0 & \ddots & 0 \\ 0 & 0 & \cdots & \varphi_n \\ \vdots & \vdots & \cdots & 0 \\ 0 & 0 & \cdots & 0 \end{bmatrix} \begin{bmatrix} u_1 \\ u_2 \\ \vdots \\ u_n \end{bmatrix} \right|\right|^2 \tag{7}$$

Here $\varphi_i,\ i = 1, \ldots, n$ are the singular values of H (diagonal terms in Σ). The Eq. (7) is equals to Eq. (8).

$$\min_x J(x) = \min_x \left(||[y_1 - \varphi_1 u_1 \quad \cdots \quad y_n - \varphi_n u_n \quad y_{n+1} \cdots \quad y_m]||^2 \right)^T \tag{8}$$

The minimum is obtained when Eq. (9) is satisfied.

$$u_i = \varphi_i^{-1} y_i, \quad i = 1, \ldots, n \tag{9}$$

Finally, from (9) and the definition $u = V^T \Delta x$, multiplying by V and using the orthogonality of V Eq. (10) is obtained.

$$\Delta x = V\, u_i \tag{10}$$

3. Numerical Observability in Distribution Systems

The observability analysis ensures that the system state variables values can be obtained from the measurement set. Then, a unique solution for the SE will be obtained. In this case, it is said that the system is observable. The observability analysis is done before running SE algorithm and its results depend on both the number of measurements and their topological location. Observability analysis is based on the inverse function theorem (16). Thus the problem $z = h(x)$ has an unique solution if, and only if, the Jacobian matrix $H(x)$ is nonsingular. This means that $H(x)$ is of full rank; then, there should be as many independent measurements as state variables in the system.

3.1 Power measurements

The DS observability is independent from both branch parameters and operational state (3). In Figure 1, the branch current is given by Eq. (11). From (11), active (P_{kl}) and reactive (Q_{kl}) power flows can be obtained. These are represented by Eqs. (12) and (13), respectively.

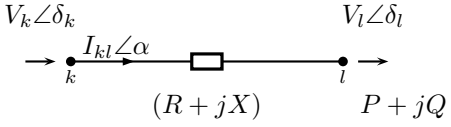

Figure 1 Radial distribution system branch

$$\tilde{I}_{kl} = \left(\frac{\tilde{S}}{\tilde{V}_l}\right)^* = \frac{P - jQ}{V_l e^{-j\delta_l}}. \tag{11}$$

where $\tilde{I}$ is the complex current, $\tilde{S}$ is the complex power, V is the voltage magnitude and δ is the voltage phase angle.

$$P_{kl} = \frac{V_k\,[R(V_k - V_l \cos\delta_{kl}) + XV_l \sin\delta_{kl}]}{R^2 + X^2} \tag{12}$$

Here R is the branch resistance, X is the branch inductive reactance and $\delta_{kl} = \delta_k - \delta_l$.

$$Q_{kl} = \frac{V_k\,[X(V_k - V_l \cos\delta_{kl}) - RV_l \sin\delta_{kl}]}{R^2 + X^2} \tag{13}$$

In DS, it is assumed that $X \approx R$. This, at first glance, suggests that it is not possible to decouple the active power from the reactive power, as it is often done in large power systems (12). However, using an orthogonal linear rotational transformation matrix T, it is possible to obtain a decoupled relationship between the state variables and power flows (17). This can be applied in DS. In this sense, the cosine is eliminated from (12) and (13), obtaining Eq. (14):

$$\sin \delta_{kl} = \frac{XP_{kl} - RQ_{kl}}{V_k V_l}. \tag{14}$$

In the same way, the sine can be eliminated, obtaining Eq. (15):

$$V_k - V_l \cos \delta_{kl} = \frac{RP_{kl} + XQ_{kl}}{V_k}. \tag{15}$$

In Figure 2, S' is the orthogonal linear rotational transformation for complex power S.

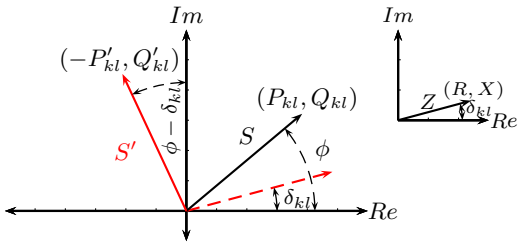

Figure 2 Complex power transformation

From Eqs. (14) and (15), a transformation matrix T is assembled. In deriving these equations, it was assumed that the voltage magnitudes are close to $1.0\ p.u.$ and each one was divided by the impedance magnitude Z. Eq. (16) provides the relationship between active and reactive power flows, and active (P'_{kl}) and reactive (Q'_{kl}) modified power flows.

$$\begin{bmatrix} P'_{kl} \\ Q'_{kl} \end{bmatrix} = T \begin{bmatrix} P_{kl} \\ Q_{kl} \end{bmatrix} = \begin{bmatrix} \frac{X}{Z} & -\frac{R}{Z} \\ \frac{R}{Z} & \frac{X}{Z} \end{bmatrix} \begin{bmatrix} P_{kl} \\ Q_{kl} \end{bmatrix} \tag{16}$$

According to the phasor diagram for Z in Figure 2, the transformation matrix T becomes as in Eq. (17):

$$T = \begin{bmatrix} \sin \delta_{kl} & -\cos \delta_{kl} \\ cos\delta_{kl} & \sin \delta_{kl} \end{bmatrix}, \tag{17}$$

with this T and the phasor diagram for S', Eqs. (18) and (19) are found as:

$$P'_{kl} = -S' \sin(\phi - \delta_{kl}), \tag{18}$$

$$Q'_{kl} = S' \cos(\phi - \delta_{kl}). \tag{19}$$

The S phasor can be rotated on the complex plane by using the transformation matrix. Applying the matrix T to (14) and (15), are obtained Eqs. (20) and (21):

$$\sin \delta_{kl} = \frac{Z\, P'_{kl}}{V_k\, V_l}, \tag{20}$$

$$V_k - V_l \cos \delta_{kl} = \frac{ZQ'_{kl}}{V_k V_l}. \tag{21}$$

In (20) and (21) it may be seen that the active modified power flow could be decoupled from the reactive modified power flow. This suggests that the observability analysis for DS's can be done in a similar way as in high voltage systems. To implement the observability analysis the transformation matrix T must be applied on each node of the DS, because the angle δ_{kl} varies for each one.

To linearize the observability analysis, the decoupled (DC) state estimation can be used. The DCSE has the same DC load flow's features (12; 13). For the DCSE in DS it is assumed:

- A flat voltage profile: $V = 1.0\ p.u.$ and $\delta = 0°$.
- The impedance magnitude is $Z = 1.0\ p.u.$.

It is assumed, for small angles ($\delta_{kl} < 10°$) that: $\sin \delta_{kl} \approx \delta_k - \delta_l$ and $\cos \delta_{kl} \approx 1$. With these conditions and using the DC load flow, the modified powers P' and Q' at node k can be written as Eqs. (22) and (23), respectively:

$$P'_k = \sum_{l \in \aleph_k} P'_{kl} = \sum_{l \in \aleph_k} (\delta_k - \delta_l), \tag{22}$$

$$Q'_k = \sum_{l \in \aleph_k} Q'_{kl} = \sum_{l \in \aleph_k} (V_k - V_l). \tag{23}$$

Where $\aleph_k$ is the set of nodes connected to node k. Eqs. (22) and (23) show the relationship between the modified DC load flow and state variables. Thus the DS is observable if there exist n independent measurements of P'_k such that the determinant of $H_{P'\delta}$ is not zero (12). Then, the DS is observable if the decoupled Jacobian matrix has full rank. In the slack node, the voltage angle is assumed as $\delta_0 = 0°$. This means that the DS is observable if inequality (24) is satisfied:

$$(H_{P'\delta}) \geqslant n - 1. \tag{24}$$

In classical state estimation analysis, the matrix formulation of (2) is written as Eq. (25). The gain matrix is defined as $G(x) = \left[[H]^T [W^{-1}][H]\right]$ and its properties provide information about the system observability (18).

$$\min_x J(x) = [z - [H]x]^T [W^{-1}][z - [H]x] \tag{25}$$

In Eq. (22) is shown, that if the modified power flow $P'_k = 0$ the state variable $\delta_{kl} = 0°$. If this condition is not satisfied,

the DS is unobservable. Using Eq. (26) one iteration of the DCSE is calculated (12; 19).

$$G_{\delta}^{0}\delta = H_{P'\delta}^{T} W_{P'}^{-1} z_{P'} \tag{26}$$

The SE for DS has an unique solution if, and only if, Eq. (26) is satisfied for δ, which is the same as G_{δ}^{0} is nonsingular. Then a radial DS is observable if the decoupled gain matrix has full rank as in Eq. (27).

$$(G_{\delta}) \geqslant n-1 \tag{27}$$

3.2 Branch Current Measurements

In large power systems, the SE uses power flow, power injection and voltage magnitude measurements (14). The line current magnitude measurements are commonly used to increase redundancy. In DS, branch current magnitude measurements are widely used, instead of power measurements.

When only magnitude measurements are available, the system can have multiple solutions for some state variables (20; 21). In the DS shown in Figure 3a, it is assumed that the region of system inside the ellipse is observable by using power flow measurements. Thus the angle δ_l is unknown and can be estimated using current and voltage magnitude measurements. The phasor diagram for the DS is shown in Figure 3b. Points p_1 and p_2 are two possible solutions for the voltage phasor $\tilde{V}_k$. In the same way, the phase angle δ_l has two possible solutions.

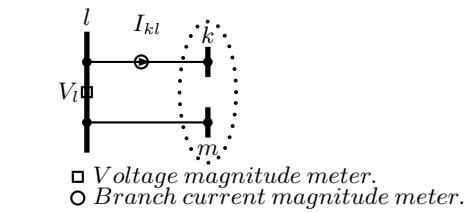

(a) Distribution system

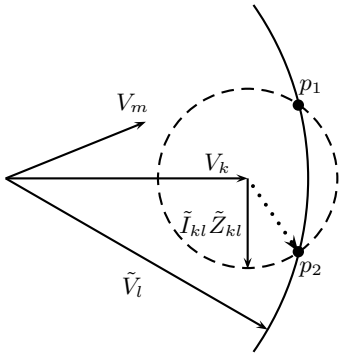

(b) Phasor diagram

Figure 3 DS and SE with two possible solutions (20)

The DS shown in Figure 3a is numerically observable because there are five state variables which are linearly independent. However, the solution is not unique due to nonlinearity.

3.3 Phasor Measurement Units

The voltage and branch current phasors can be measured with a PMU (22). The branch current phase angle α_{ln} is measured with respect to the voltage phase angle at slack node k. The PMU is synchronized respect to cosine function at the system's nominal frequency (7).

In radial DS, shown in Figure 4a, branch current phasors are chosen as state variables: $\begin{bmatrix}\alpha_{kl} & \alpha_{lm} & \alpha_{ln} & I_{kl} & I_{lm} & I_{ln}\end{bmatrix}$. To measure a branch current phasor, a PMU is used. With conventional measurements and the PMU, this DS is numerically observable because there are as many independent pairs of measurements of P and Q as branches. Here the PMU increases the redundancy.

In the DS shown in Figure 4b, it is assumed that the power flow measurement at node n has been removed and the PMU is placed at node l. Thus, the active and reactive power injections at node l are known. Then the Jacobian matrix becomes in Eq. (28):

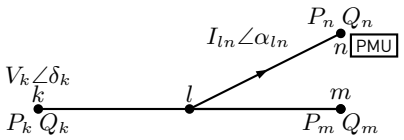

(a) PMU as a redundant measurement

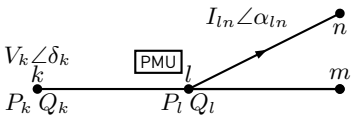

(b) PMU as a critical measurement

Figure 4 Radial distribution system with a PMU

$$H_{\alpha,I} = \begin{bmatrix} \frac{\partial P_k}{\partial \alpha_{kl}} & 0 & 0 & \frac{\partial P_k}{\partial I_{kl}} & 0 & 0 \\ 0 & \frac{\partial P_l}{\partial \alpha_{lm}} & \frac{\partial P_l}{\partial \alpha_{ln}} & 0 & \frac{\partial P_l}{\partial I_{lm}} & \frac{\partial P_l}{\partial I_{ln}} \\ \frac{\partial Q_k}{\partial \alpha_{kl}} & 0 & 0 & \frac{\partial Q_k}{\partial I_{kl}} & 0 & 0 \\ 0 & \frac{\partial Q_l}{\partial \alpha_{lm}} & \frac{\partial Q_l}{\partial \alpha_{ln}} & 0 & \frac{\partial Q_l}{\partial I_{lm}} & \frac{\partial Q_l}{\partial I_{ln}} \\ 0 & 0 & 1 & 0 & 0 & 0 \\ 0 & 0 & 0 & 0 & 0 & 1 \end{bmatrix}, \tag{28}$$

and the system gain matrix is the Eq. (29).

$$G_{\alpha,I}=\begin{bmatrix}
\left(\frac{\partial P_k}{\partial \alpha_{kl}}\right)^2+\left(\frac{\partial Q_k}{\partial \alpha_{kl}}\right)^2 & 0 & 0 & \frac{\partial P_k}{\partial \alpha_{kl}}\frac{\partial P_k}{\partial I_{kl}}+\frac{\partial Q_k}{\partial \alpha_{kl}}\frac{\partial Q_k}{\partial I_{kl}} & 0 & 0\\
0 & \left(\frac{\partial P_l}{\partial \alpha_{lm}}\right)^2+\left(\frac{\partial Q_l}{\partial \alpha_{lm}}\right)^2+1 & \frac{\partial P_l}{\partial \alpha_{lm}}\frac{\partial P_l}{\partial \alpha_{ln}}+\frac{\partial Q_l}{\partial \alpha_{lm}}\frac{\partial Q_l}{\partial \alpha_{ln}} & 0 & \frac{\partial P_l}{\partial \alpha_{lm}}\frac{\partial P_l}{\partial I_{lm}}+\frac{\partial Q_l}{\partial \alpha_{lm}}\frac{\partial Q_l}{\partial I_{lm}} & \frac{\partial P_l}{\partial \alpha_{lm}}\frac{\partial P_l}{\partial I_{ln}}+\frac{\partial Q_l}{\partial \alpha_{lm}}\frac{\partial Q_l}{\partial I_{ln}}\\
0 & \frac{\partial P_l}{\partial \alpha_{lm}}\frac{\partial P_l}{\partial \alpha_{ln}}+\frac{\partial Q_l}{\partial \alpha_{lm}}\frac{\partial Q_l}{\partial \alpha_{ln}} & \left(\frac{\partial P_l}{\partial \alpha_{ln}}\right)^2+\left(\frac{\partial Q_l}{\partial \alpha_{ln}}\right)^2 & 0 & \frac{\partial P_l}{\partial \alpha_{ln}}\frac{\partial P_l}{\partial I_{lm}}+\frac{\partial Q_l}{\partial \alpha_{ln}}\frac{\partial Q_l}{\partial I_{lm}} & \frac{\partial P_l}{\partial \alpha_{ln}}\frac{\partial P_l}{\partial I_{ln}}+\frac{\partial Q_l}{\partial \alpha_{ln}}\frac{\partial Q_l}{\partial I_{ln}}\\
\frac{\partial P_k}{\partial \alpha_{kl}}\frac{\partial P_k}{\partial I_{kl}}+\frac{\partial Q_k}{\partial \alpha_{kl}}\frac{\partial Q_k}{\partial I_{kl}} & 0 & 0 & \left(\frac{\partial P_k}{\partial I_{kl}}\right)^2+\left(\frac{\partial Q_l}{\partial I_{kl}}\right)^2 & 0 & 0\\
0 & \frac{\partial P_l}{\partial \alpha_{lm}}\frac{\partial P_l}{\partial I_{lm}}+\frac{\partial Q_l}{\partial \alpha_{lm}}\frac{\partial Q_l}{\partial I_{lm}} & \frac{\partial P_l}{\partial \alpha_{ln}}\frac{\partial P_l}{\partial I_{lm}}+\frac{\partial Q_l}{\partial \alpha_{ln}}\frac{\partial Q_l}{\partial I_{lm}} & 0 & \left(\frac{\partial P_l}{\partial I_{lm}}\right)^2+\left(\frac{\partial Q_l}{\partial I_{lm}}\right)^2+1 & \frac{\partial P_l}{\partial I_{lm}}\frac{\partial P_l}{\partial I_{ln}}+\frac{\partial Q_l}{\partial I_{lm}}\frac{\partial Q_l}{\partial I_{ln}}\\
0 & \frac{\partial P_l}{\partial \alpha_{lm}}\frac{\partial P_l}{\partial I_{ln}}+\frac{\partial Q_l}{\partial \alpha_{lm}}\frac{\partial Q_l}{\partial I_{ln}} & \frac{\partial P_l}{\partial \alpha_{ln}}\frac{\partial P_l}{\partial I_{ln}}+\frac{\partial Q_l}{\partial \alpha_{ln}}\frac{\partial Q_l}{\partial I_{ln}} & 0 & \frac{\partial P_l}{\partial I_{lm}}\frac{\partial P_l}{\partial I_{ln}}+\frac{\partial Q_l}{\partial I_{lm}}\frac{\partial Q_l}{\partial I_{ln}} & \left(\frac{\partial P_l}{\partial I_{ln}}\right)^2+\left(\frac{\partial Q_l}{\partial I_{ln}}\right)^2
\end{bmatrix} \tag{29}$$

The gain matrix ($G_{\alpha,I}$), is nonsingular, because its determinant is not zero, as can be checked in Eq. (30).

$$\det(G_{\alpha,I})=\left(\frac{\partial P_k}{\partial \alpha_{kl}}\frac{\partial Q_k}{\partial I_{kl}}-\frac{\partial P_k}{\partial I_{kl}}\frac{\partial Q_k}{\partial \alpha_{kl}}\right)^2\left(\frac{\partial P_l}{\partial I_{ln}}\frac{\partial Q_l}{\partial \alpha_{ln}}-\frac{\partial P_l}{\partial \alpha_{ln}}\frac{\partial Q_l}{\partial I_{ln}}\right)^2 \tag{30}$$

The branch current magnitude and phase angle are linearly independent such as the power injection measurements at the nodes k and l. Consequently, the system is numerically observable and the branch current phasor is a critical measurement. If the PMU is removed from the measurement set, the system will be unobservable (22).

In short, the solution for the SE is unique when the branch current phase angle α_{kl} is known. See the dashed phasor in the phasor diagram shown in Figure 3b.

4. State Estimation Algorithm

Observability results for DS can be applied to an SE. In this way, an SE algorithm is proposed. It was developed to include branch current phase angle measurements. The state variables are the branch current phasors. These variables are used to compute voltage phasors. Distribution transformers and multiple power sources were modeled. The SE algorithm is based on (23; 24).

4.1 Measurement Equations

The SE uses conventional DS measurements and PMUs. Conventional measurements are: power flows, power injections, voltage magnitudes and branch current magnitudes. Branch current phase angle measurement is also used. To ensure both system observability and an unique solution, pseudo-measurements can be included. The Jacobian matrix is assembled from Eqs. (31), (32), (33) and (34).

- Branch power measurements

$$P_{kl}+jQ_{kl}=V_kI_{kl}\left[\cos(\delta_k-\alpha_{kl})+j\sin(\delta_k-\alpha_{kl})\right]. \tag{31}$$

- Power injection measurements

$$P_k+jQ_k=\tilde{V}_k\left(\sum_{i=1}^{m}\tilde{I}_{ik}-\sum_{i=m+1}^{n}\tilde{I}_{ki}\right)^*. \tag{32}$$

- Voltage magnitude measurements

$$\tilde{V}_{n+1}=\tilde{V}_0-\sum_{i=1}^{n+1}\tilde{I}_{i-1,i}\tilde{Z}_{i-1,i}. \tag{33}$$

- Branch current phasor measurements

$$I_{kl}\angle\alpha_{kl}=I_{kl}\angle\alpha_{kl}. \tag{34}$$

The SE is summarized in Algorithm 1. The convergence is reached by using Newton Raphson's method.

Algorithm 1: State estimator

Flat voltages $1\angle 0°$
$t\leftarrow 0$
Compute branch currents x^0
while $\max(|\Delta x^t|)>\xi$ **do**
  Compute: phasor voltages, H and $W^{-\frac{1}{2}}H$;
  SVD of $W^{-\frac{1}{2}}H$ as $U\Sigma V^T$;
  Calculate residuals $\Delta z^t=z-f(x^t)$;
  Solve: $\Delta x^t=V\varphi^{-1}U^TW^{-1}\Delta z^t$;
  Update state $x^{t+1}=x^t+\Delta x^t$;
end

5. Test Results

In this section, the SE algorithm results are analyzed. To validate the SE, one hundred replications of the estimation

were simulated and the results averaged. The DS used is the IEEE 13 nodes test feeder, to which a DGEN can be connected. In the simulation, different measurements sets were used and observability analysis results were applied. The load flow solution for the DS and DGEN was run in PSE ®. This solution is taken as the real value of the state variables. The data of the IEEE 13 nodes test feeder were used as measurements, by adding a random noise signal. The noise is the simulated error in measurements and was assumed normally distributed. For the measurements, the maximum error can be up to $\pm 6\%$ of the exact value. For the pseudo-measurements, the maximum error can be up to $\pm 45\%$ of the exact value. All the algorithms were simulated in Matlab ®.

5.1 Distribution Systems State Estimation Performance

The single phase diagram for the DS and the DGEN is shown in Figure 5. The DGEN is the part inside the ellipse. The external network is composed of four loads and a power transformer. The DG is a synchronous generator. A Diesel engine is the generator prime mover. In the simulation, power measurements in the DS at nodes, slack and 10th are assumed. The latter is the point of common coupling (PCC). In the DGEN measurements in both the load nodes and the generation node are considered. In the remaining nodes, power pseudo-measurements are assumed. The voltage magnitude measure is considered only at the slack node. This measurement increases the redundancy.

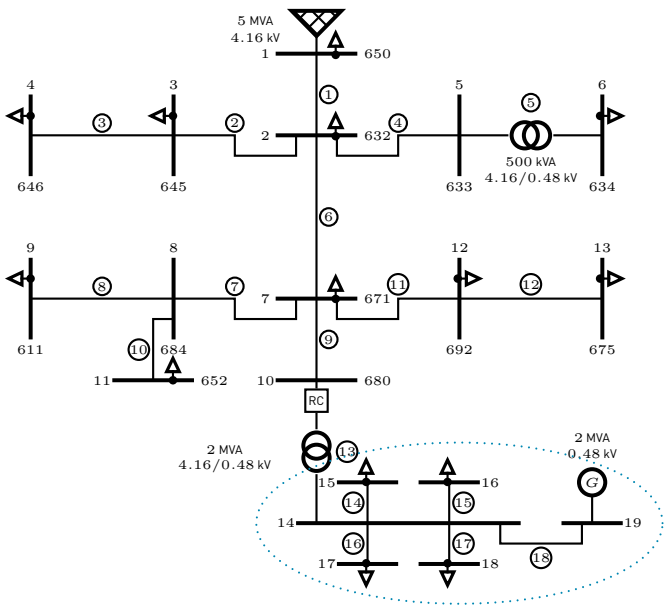

Figure 5 Modified IEEE 13 nodes test feeder, DG and external network

Power Measurements

The branch current phasors were estimated with a set formed by n pairs of power measurements and power pseudo-measurements. In Figure 6a, a histogram for the voltage magnitude errors is shown. The absolute error is less than 0.5% for all nodes of the system.

In the test system, the voltage angle is very small (ie. $-2^\circ \leq \delta \leq 0^\circ$), thus the difference between real and estimated values can result in large errors, mainly in those nodes where the voltage phase angle is close to 0°. In Figure 6b it is shown the histogram of the difference between real and estimated voltage phase angles. This difference is less than $|0.25|^\circ$.

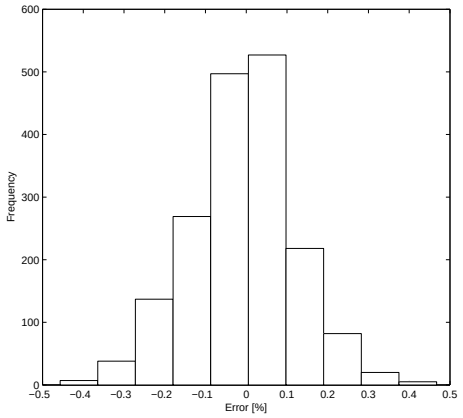

(a) Voltage magnitude error

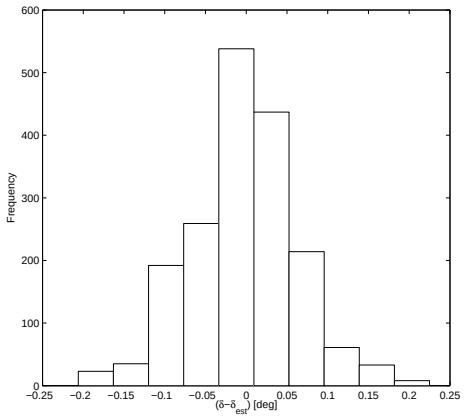

(b) Voltage phase angle difference

Figure 6 Histogram, n pairs of power measurements and pseudo-measurements

For the next analysis, in the test system, the power pseudo-measurements at node 7 were removed. In this case, the system has as many measurements as branches (ie. $n-1$ pairs of power measurements). Figure 7 shows

the histogram for the voltage magnitude error and the voltage phase angle difference. Despite the fact that the measurement set has fewer measures than in the previous case, the results are similar since the voltage magnitude error is less than $|0.5|\%$ (Figure 7a), and the difference between real and estimated voltage phase angle is less than $|0.25|^\circ$ (Figure 7b).

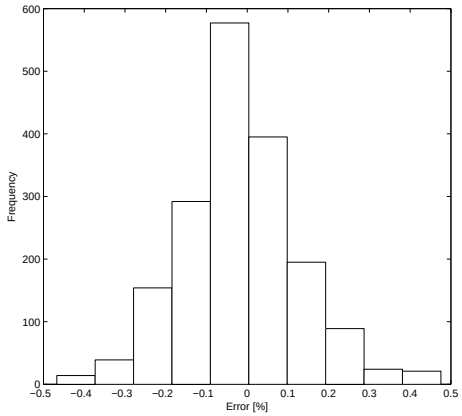

(a) Voltage magnitude error

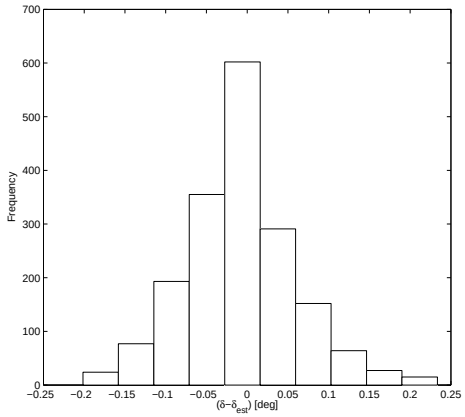

(b) Voltage phase angle difference

Figure 7 Histogram, $(n-1)$ pairs of power measurements and pseudo-measurements

Phasor Measurements Units

From the observability analysis in a radial DS, two pairs of P and Q measurements can be replaced by a PMU, if it is located in the previous node (l), see Figure 4b. Thus, the PMU must measure both, the power injected and the branch current phasor in one of the existing branches between node (l) and downstream nodes (m or n).

By adding a PMU to measure the branch current phasor, there exist as many pairs of measurements as branches in the system; in consequence, all measurements are critical. In figure 5, a PMU has been connected at node 2. In nodes 5 and 6 it is assumed that there are no measurements or pseudo-measurements. The Figure 8 shows the histogram for the voltage magnitude error and voltage phase angle difference.

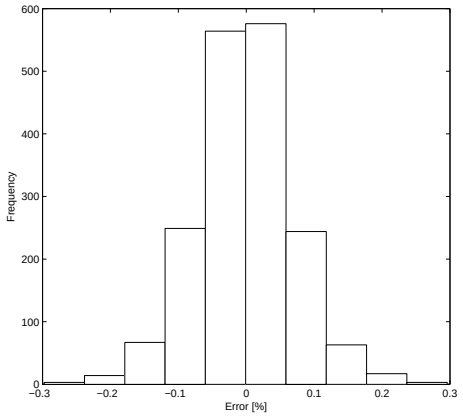

(a) Voltage magnitude error

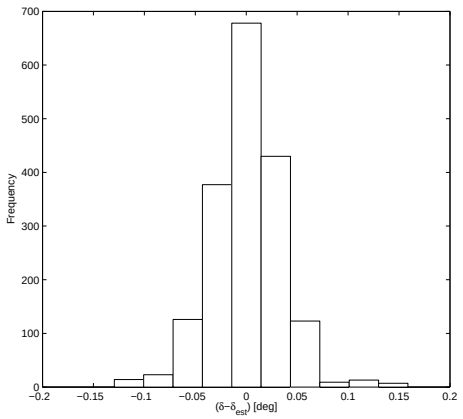

(b) Voltage phase angle difference

Figure 8 Histogram, PMU in the measurements set

When the PMU is included, the accuracy of the SE increases, because the voltage magnitude error decreased from $|0.5|\%$ to $|0.3|\%$ and the difference in voltage phase angle is in the range $-0.15^\circ \leq \delta - \delta_{est} \leq 0.20^\circ$. Table 1 shows the maximum absolute average error when the PMU is used. This reduction is, undoubtedly, due mainly to the fact that the PMU has a lower inherent error, with a standard deviation $\sigma_{mag} = 0.00067$ and $\sigma_{ang} = 0.00097$, compared to the values of the conventional measurement that has $\sigma = 0.0125$. Nevertheless, the errors are smaller.

To study the influence of the PMU location in the SE performance, the location was changed, keeping the

Table 1 Maximum average error in SE using a PMU

variable	node	$\lvert\%\rvert$ error
V	3	0.0124
δ	5	0.4355

configuration shown in Figure 4b. The noise in the measurements and pseudo-measurements was increased to values close to the maximum allowed $\pm 6\%$ and $\pm 45\%$ respectively. The maximum error is summarized in the Table 2.

Table 2 Maximum error when PMU location is changed

Node and branch with PMU	Nodes without measures	Error $\%V$	Error $\%\delta$
2, (6)	5, 7	0.0082	0.5277
2, (4)	3, 5	0.0278	4.0512
7, (11)	10, 12	0.0188	2.3379
8, (10)	9, 11	0.7946	4.1038

Figure 9 shows the average error of the state variables, when the PMU location is changed. Both voltage magnitude and phase angle, obtained with the proposed SE, were influenced by the PMU location. For all measurement sets, the voltage phase angle at the generation node presents the greatest deviation compared to all other nodes in the system, as shown in Figure (9b). When the PMU is located at node 8, the downstream nodes (9 and 11) have the greater errors for the voltage magnitude and phase angle as shown in Table (2).

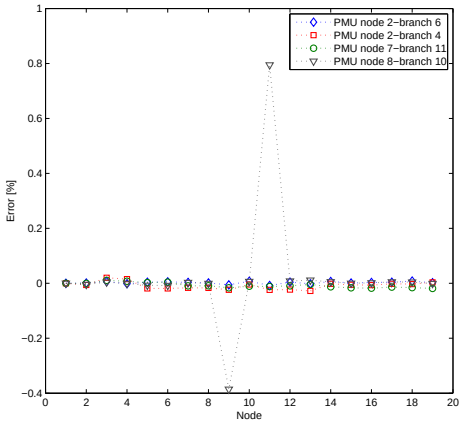

(a) Voltage magnitude error

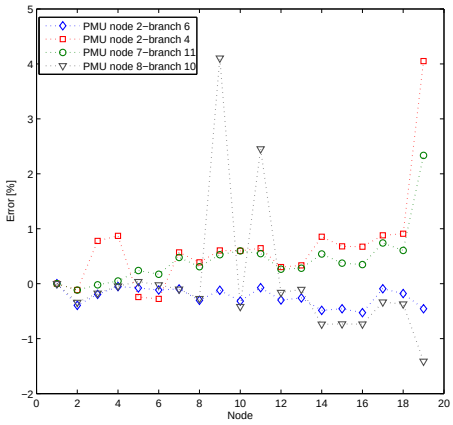

(b) Voltage phase angle error

Figure 9 Error when PMU location is changed

5.2 State Estimation Applications to Distributed Generation

The SE outputs are used to compute the system total losses. Thus, the DS behavior could be assessed when DGEN is connected as a new load. In the same way, the SE data are used to implement another proposed algorithm to re-synchronize the DGEN to the DS, this algorithm can be used as a MG self-healing function.

Prediction of Losses

The total DS losses can be estimated using the SE results. Figure 10 shows the total DS loss histogram. Active and reactive power loss errors are less than 8%. This percentage is an acceptable value especially taking into account that the pseudo-measurement error can be as large as $\pm 45\%$.

Distributed Generation Re-synchronization

The DG has the ability to operate in grid and off-grid mode. One of the main challenges in off-grid mode operation is re-synchronization with an external system (25). This is a necessary condition to change operation from off-grid to grid mode. If voltages at the PCC are not synchronized when the switch is closed, high currents can occur, affecting the power quality in both DS and DG grid (8; 6). For the simulation, the DG is composed by a Diesel generator. In off-grid mode the DG feeds an external network (DGEN).

To re-synchronize the DGEN to the DS, it is assumed that the DGEN was connected to the DS. Next, the DGEN is removed from the DS and starts to operate in off-grid mode. Then, the DGEN can be re-synchronized to the DS. Under these conditions the DGEN re-synchronization is carried out at the PCC.

For re-synchronization, generation control was assumed as a proportional integral derivative controller. Both synchronous Diesel generator and governor parameters

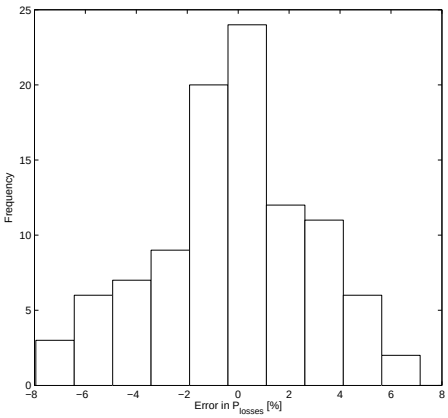

(a) Active power losses error

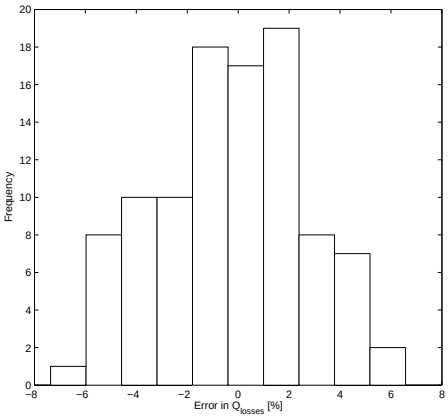

(b) Reactive power losses error

Figure 10 Histogram for estimated power losses

were taken from (26). The generator impedances were adjusted to 60 Hz. The automatic voltage regulator (AVR) is a modification of IEEE AC4 model. For each controller, block diagrams are shown in Figures 11 and 12. In the synchronization, the AVR reference is modified in accordance with the estimated state variables. The governor holds the frequency in the DGEN constant.

Figure 13a shows the voltage magnitude and angle at the PCC, in the DS and the DGEN sides (see Figure 5). The voltage magnitude difference is $V_{kl} = 0.0615\, p.u.$, and the voltage phase angle difference is $\delta_{kl} > 10°$. For the DG rating, the restrictions of the Standard IEEE 1547 (27) are not satisfied. Since, for a 2 [MVA] generator the maximum allowed differences are $V_{kl} < 3\%$ and $\delta_{kl} < 10°$. The synchronous machine variables in off-gride mode are shown in Figure 13b, the voltage magnitude is $1.0\, p.u.$ and phase angle is $0°$.

The re-synchronization process is described as follows:

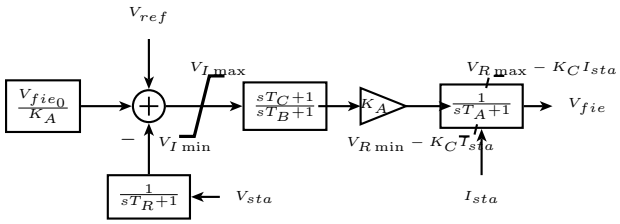

Figure 11 Block diagram automatic voltage regulator

the estimated value for the voltage phasor at node 10, is the reference value to synchronize the DG. With these values the voltage phasor at the generation node in the DGEN may be computed, using (33); to this phasor the transformer phase angle must be added. The synchronous machine must be controlled until the conditions of the standard (27) are satisfied. Then, the RC, at the PCC, could be closed.

Figure 14a shows the voltage phasors in both sides, at the PCC, before, during and after the connection between the DGEN and DS. It is observed that restrictions were satisfied for both the voltage magnitude and phase angle difference. In the Figure 14b is shown, the reference voltage phasor at the generation node, in DGEN. This phasor is $0.935\angle - (3 + 30)\circ$, because the power transformer vector group is ΔY11.

For reference, Figure 15a shows the branch current and frequency during the re-synchronization. At the PCC, the branch current was close to load currents 13 [A]. In the DGEN the frequency was stable, because the variation is below to $\Delta f < 0.1$ Hz, thus, the standard (27) frequency requirements are reached.

When the DGEN and DS are coupled, the system reliability improves. For example, if the generator in the DGEN has enough capacity, it is possible to export active and reactive power to DS. This task can be fulfilled with the synchronous machine control in the DGEN. The active and reactive power in both sides of the system are shown in Figure 16b. After the connection, both sources continue feeding their own loads. When the voltage phase reference in the AVR is changed to 1.0 p.u., the DGEN exports reactive power to DS. Similarly, an increase in active power generation in the DGEN can be exported to DS. These changes in the reference parameters for the generation in the DGEN, lead to an improved voltage profile of the system, as shown in Figure 16a.

6. Conclusions

With the use of PMUs in radial DS, the system observability can be ensured, if there are enough pairs of P and Q measurements.

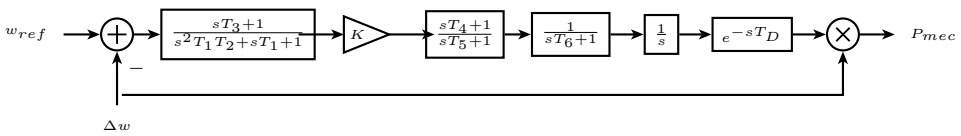

Figure 12 Block diagram governor

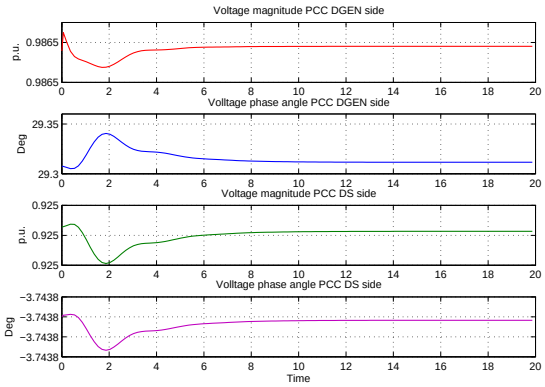

(a) Voltage phasors

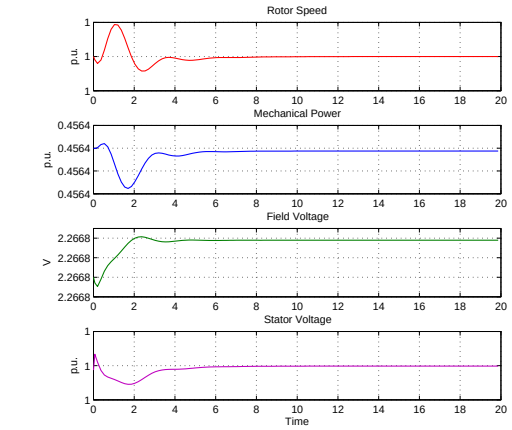

(b) Generator response

Figure 13 DG in off-grid mode

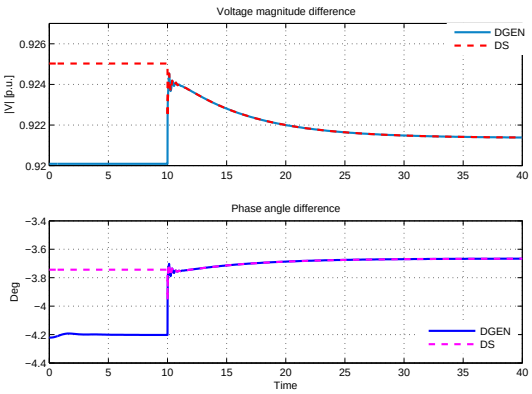

(a) Voltage phasors

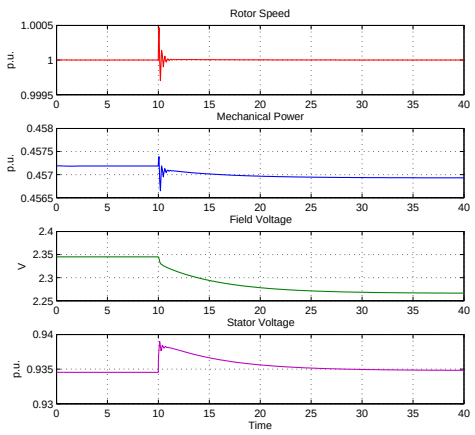

(b) Generator response

Figure 14 DS and DG in off-grid and grid mode

In this way, the PMU location must contribute to increase the redundancy in the measurements set. In the simulation the proposed SE algorithm was robust for the estimation of voltage magnitudes, because the solution is not significantly affected by the measurements set or by their location. Thus, the voltage phase angle is estimated with enough precision in almost all nodes of the system. As the system phase angles approach zero, significant percentage deviations may occur.

The SE results suggest, that if the branch current phasor is measured in the main feeder, the SE errors decrease, especially at the nodes that are located downstream the PMU.

The SE can be used to assess system total losses and to improve the re-synchronization of synchronous machines. This last is a MGs self-healing function and can be implemented in those MGs that use synchronous generators.

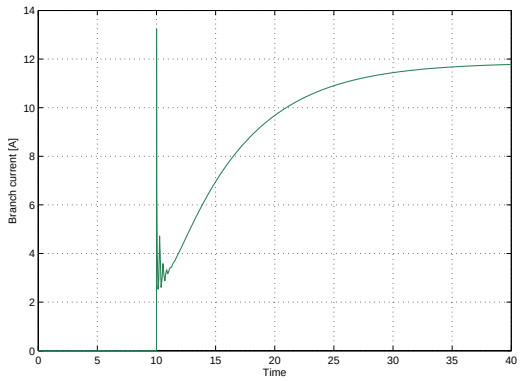

(a) Branch current at the PCC

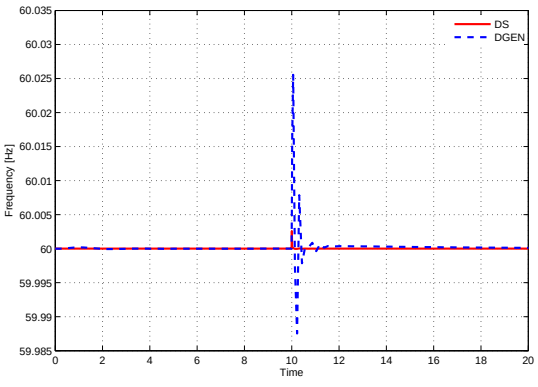

(b) System frequency

Figure 15 Branch current and frequency during the re-synchronization

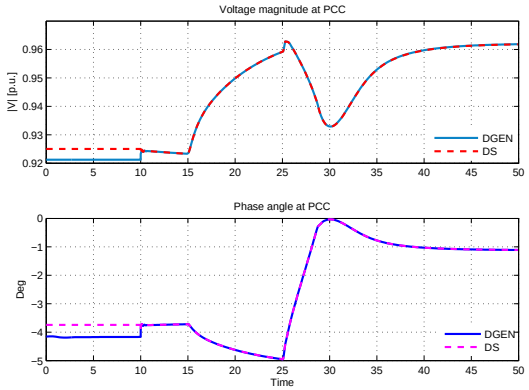

(a) Voltage phasor

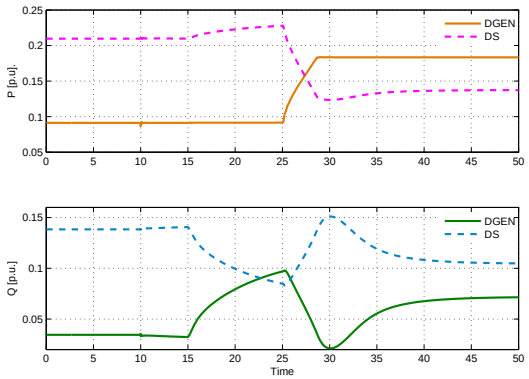

(b) Active and reactive power

Figure 16 Active and reactive power exports from DGEN

7. References

[1] C. M. Colson, M. H. Nehrir, and R. W. Gunderson, "Distributed multi-agent microgrids: a decentralized approach to resilient power system self-healing," in *4th International Symposium on Resilient Control Systems*, Boise, USA, 2011, pp. 83–88.

[2] A. Gómez-Expósito, A. Abur, A. de la Villa Jaen, and C. Gómez-Quiles, "A multilevel state estimation paradigm for smart grids," *Proceedings of the IEEE*, vol. 99, pp. 952–976, 2011.

[3] S. Choi and A. P. S. Meliopoulos, "Effective real-time operation and protection scheme of microgrids using distributed dynamic state estimation," *IEEE Transactions on Power Delivery*, vol. 32, pp. 504–514, 2017.

[4] Y. F. Huang, S. Werner, J. Huang, N. Kashyap, and V. Gupta, "State estimation in electric power grids: Meeting new challenges presented by the requirements of the future grid," *IEEE Signal Processing Magazine*, vol. 29, pp. 33–43, 2012.

[5] D. A. Haughton and G. T. Heydt, "A linear state estimation formulation for smart distribution systems," *IEEE Transactions on Power Systems*, vol. 28, pp. 1187–1195, 2013.

[6] Z. Wang, B. Chen, J. Wang, and C. Chen, "Networked microgrids for self-healing power systems," *IEEE Transactions on Smart Grid*, vol. 7, pp. 310–319, 2016.

[7] G. N. Korres and N. M. Manousakis, "State estimation and observability analysis for phasor measurement unit measured systems," *IET Generation, Transmission Distribution*, vol. 6, pp. 902–913, 2012.

[8] C. Cho, J. H. Jeon, J. Y. Kim, S. Kwon, K. Park, and S. Kim, "Active synchronizing control of a microgrid," *IEEE Transactions on Power Electronics*, vol. 26, pp. 3707–3719, 2011.

[9] F. Mahmood, H. Hooshyar, J. Lavenius, A. Bidadfar, P. Lund, and L. Vanfretti, "Real-time reduced steady-state model synthesis of active distribution networks using pmu measurements," *IEEE Transactions on Power Delivery*, vol. 32, pp. 546–555, 2017.

[10] S. R. Samantaray, I. Kamwa, and G. Joos, "Phasor measurement unit based wide-area monitoring and information sharing between micro-grids," *IET Generation, Transmission Distribution*, vol. 11, pp. 1293–1302, 2017.

[11] R. E. Larson, W. F. Tinney, and J. Peschon, "State estimation in power systems part i: Theory and feasibility," *IEEE Transactions on Power Apparatus and Systems*, vol. PAS-89, pp. 345–352, 1970.

[12] A. Monticelli and F. F. Wu, "Network observability: Theory," *IEEE Power Engineering Review*, vol. PER-5, no. 5, pp. 1042–1048, 1985.

[13] A. J. Wood and B. F. Wollenberg, *Power generation, operation, and control*, 1st ed. New York, USA: John Wiley & Sons, 1984, pp. 391–426.

[14] A. Abur and A. Gómez Expósito, *Power system state estimation: theory and implementation*, 1st ed. New York, USA: Marcel Dekker, Inc., 2004.

[15] C. Madtharad, S. Premrudeepreechacharn, and N. R. Watson, "Power system state estimation using singular value decomposition," *Electric Power Systems Research*, vol. 67, pp. 99–107, 2003.

[16] T. S. Lee, "Numerical aspects of the inverse function theory," in *The 22nd IEEE Conference on Decision and Control*, Lexington, USA, 1983, pp. 424–429.

[17] R. Gelagaev, P. Vermeyen, J. Vandewalle, and J. Driesen, "Numerical observability analysis of distribution systems," in *Proceedings of 14th International Conference on Harmonics and Quality of Power - ICHQP*, 2010, pp. 1–6.

[18] F. C. Schweppe and E. J. Handschin, "Static state estimation in electric power systems," *Proceedings of the IEEE*, vol. 62, pp. 972–982, 1974.

[19] A. Monticelli and F. F. Wu, "Network observability: Identification of observable islands and measurement placement," *IEEE Power Engineering Review*, vol. PER-5, pp. 1035–1041, 1985.

[20] A. Abur and A. G. Expósito, "Algorithm for determining phase-angle observability in the presence of line-current-magnitude measurements," *IEE Proceedings - Generation, Transmission and Distribution*, vol. 142, pp. 453–458, 1995.

[21] J. M. R. Muñoz and A. G. Expósito, "A line-current measurement based state estimator," *IEEE Transactions on Power Systems*, vol. 7, no. 2, pp. 513–519, 1992.

[22] M. Göl and A. Abur, "Observability and criticality analyses for power systems measured by phasor measurements," *IEEE Transactions on Power Systems*, vol. 28, pp. 3319–3326, 2013.

[23] H. Wang and N. N. Schulz, "A revised branch current-based distribution system state estimation algorithm and meter placement impact," *IEEE Transactions on Power Systems*, vol. 19, pp. 207–213, 2004.

[24] M. E. Baran and A. W. Kelley, "A branch-current-based state estimation method for distribution systems," *IEEE Transactions on Power Systems*, vol. 10, pp. 483–491, 1995.

[25] D. Shi, Y. Luo, and R. K. Sharma, "Active synchronization control for microgrid reconnection after islanding," in *5th IEEE PES Innovative Smart Grid Technologies, Europe*, Istanbul, Turkey, 2014, pp. 1–6.

[26] J. L. Agüero, M. C. Beroqui, F. Issouribehere, and C. E. Biteznik, "Ensayos de campo y determinación de modelos de motogeneradores," in *XIII Encuentro Regional Iberoamericano de CIGRE*, Misiones, Argentina, 2009, pp. 1–8.

[27] *IEEE Application Guide for IEEE Std 1547^{TM}, IEEE Standard for Interconnecting Distributed Resources with Electric Power Systems*, Institute of Electrical and Electronics Engineers, IEEE Std 1547.2-2008, 2009.